GA–A26820

ROLE OF ECH AND ECCD IN HIGH-PERFORMANCE STEADY-STATE SCENARIOS

by
T.C. LUCE

JUNE 2010

GENERAL ATOMICS

DISCLAIMER

GA–A26820

ROLE OF ECH AND ECCD IN HIGH-PERFORMANCE STEADY-STATE SCENARIOS

by
T.C. LUCE

This is a preprint of an invited paper presented at the 16th Joint Workshop on Electron Cyclotron Emission and Electron Cyclotron Resonant Heating, April 12–15, 2010, in Sanya, China, and to be printed in the *Proceedings*.

Work supported by
the U.S. Department of Energy
under DE-FC02-04ER54698

GENERAL ATOMICS PROJECT 30200
JUNE 2010

ROLE OF ECH AND ECCD IN HIGH-PERFORMANCE STEADY-STATE SCENARIOS

T.C. LUCE
General Atomics, PO Box 85608, San Diego, California 92186-5608, USA

The ability to control the location and localization of energy and current deposition in fusion plasmas with electron cyclotron waves is unmatched by any other auxiliary heating and current drive method. The establishment of the physics basis of the wave propagation and absorption allows accurate prediction of the deposition given the launcher optics and the profiles of magnetic field, electron density, electron temperature, and impurity density. This, along with the development of the technology of high-power millimeter-wave sources and the means to transmit them to the plasma, has facilitated experiments in present-day fusion devices to demonstrate the utility of heating and current drive with electron cyclotron waves (ECH and ECCD, respectively). Three primary roles are envisioned for ECH or ECCD in burning plasmas. First, all burning plasma scenarios require some access conditions, whether it is merely heating the plasma to fusion-relevant conditions or generating specific profiles of the magnetic field necessary to access steady-state operation in a tokamak. Second, tokamak-based steady-state scenarios require efficient auxiliary current drive to sustain the magnetic configuration. Finally, control of the operating point of a burning plasma is essential. This role includes applications such as burn control, response to off-normal events, and active control of plasma instabilities. Each of these roles will be discussed using examples from present-day tokamak and stellarator experiments. Prospects for application in ITER and fusion power plants will also be presented.

1. Introduction

The use of fusion energy to satisfy the world's fundamental energy needs is an attractive long-term vision. Within the range of possible fusion energy systems, steady-state operation of magnetic confinement systems is an attractive option [1,2]. The schemes for realizing steady-state magnetic confinement fusion that are closest to achieving the conditions necessary for fusion energy production are the stellarator and the tokamak [3].

Both schemes start with a strong toroidal magnetic field. But such a field alone cannot confine plasma due to charge separation [1]. In both cases, a helical field is applied to prevent charge separation and provide plasma confinement. The two schemes apply the helical field in very different ways. In

the stellarator, the magnetic configuration is generated dominantly (in many cases, solely) by external coils that are arranged in a three-dimensional configuration. With proper design, this results in closed flux surfaces and plasma confinement. As long as the coils are energized, the magnetic configuration can be sustained and steady-state operation is possible. In the tokamak, the helical field is generated by a toroidal current flowing in the plasma. Typically, this is achieved by means of induction, so the magnetic configuration cannot be maintained in steady-state. However, noninductive means of generating currents in tokamaks are well-established [4] and fully noninductive operation has been achieved on several tokamaks [1].

Three general issues arise for steady-state magnetic fusion energy systems — accessing the steady-state fusion energy regime, sustaining that regime, and control of the operating point in normal and off-normal conditions. The theme of this paper is that advances in the technology and physics of electron cyclotron heating (ECH) and current drive (ECCD) establish the basis, both theoretically and experimentally, to address these issues. The focus here will be on the physics aspects; the technology aspects will be reviewed in other contributions to these proceedings [5].

The outline for the remainder of this paper is as follows. The fundamental aspects of ECH and ECCD — wave propagation and absorption, and the plasma response to the absorption — will be reviewed briefly with emphasis on experimental verification. Then the role of ECH and ECCD in addressing the three general steady-state issues for stellarators and tokamaks will be discussed in turn. Finally, a brief discussion of the prospects for ECH and ECCD playing a role in the steady-state operation of the next generation of magnetic confinement fusion devices will be given, along with some conclusions.

2. Validation of Basic EC Wave Physics in Plasmas

Propagation of electromagnetic waves with frequency near the electron cyclotron frequency is described well by the dispersion relations derived from cold plasma theory [6,7]. (Electron Bernstein waves, electrostatic waves in this same frequency range, will not be considered here.) Two wave polarizations are supported by the plasma, with distinct dispersion relations. In the limit of propagation perpendicular to the plasma magnetic field, the two polarizations correspond to waves with the wave electric field parallel (O mode) and perpendicular (X mode) to the plasma magnetic field. In the limit of propagation parallel to the plasma magnetic field, these become left-handed and right-handed circularly polarized, respectively. They are commonly referred to by O mode

and X mode independent of the direction of propagation. The O mode propagates when the wave frequency is above the electron plasma frequency $\omega_p \equiv \left(ne^2/\varepsilon_0 m\right)^{1/2}$, while the X mode propagates above the right-hand cutoff, which is a combination of the electron cyclotron frequency and the electron plasma frequency

$$\omega_{rh} \equiv \left(\Omega/2\right)\left[1+\sqrt{1+4\left(\omega_p^2/\Omega^2\right)}\right] \quad ,$$

where $\Omega \equiv eB/m$ is the gyrofrequency. With these dispersion relations, the propagation of the waves is predicted accurately by ray tracing using WKB theory [8]. The physics of absorption by the electron cyclotron resonance is long developed [9] and has been validated extensively. An example of experimental validation of the propagation and absorption physics from the DIII-D tokamak is shown in Fig. 1 [10]. Waves at 110 GHz with mixed O and X mode polarization are launched at an oblique angle with respect to the major radius from side where the magnetic field is lower, as shown in the left figure. The lines in the figure are projections of the predicted paths of propagation projected back on the poloidal cross-section of the launch point. The density and magnetic field are such that both polarizations experience significant refraction away from the trajectory predicted in vacuum. The right figure shows the amplitude response of the electron cyclotron emission measurement of the electron temperature when the power is modulated with a square wave of 50% duty cycle. The peaks are broadened by heat transport in the plasma, but it is clear that the peaks correspond to the locations predicted by the ray tracing code, including a hint of the second pass through the resonance for the X mode and the strong absorption on the second pass of the O mode. This correspondence requires both the propagation and absorption to be correctly predicted. This is merely one example of a extensive set of experimental validations of the basic theory of electron cyclotron wave propagation and absorption [11].

Perhaps the most stringent test of the theory is in the prediction of the plasma response in cases where the electron cyclotron waves are predicted to drive substantial current in the plasma. As mentioned above, the ability to drive current noninductively is essential to steady-state operation of a tokamak. The current arises because the absorption can occur in a very localized region in both real space and velocity space due to the resonance condition $\omega = \ell\Omega/\gamma + k_{||}v_{||}$,

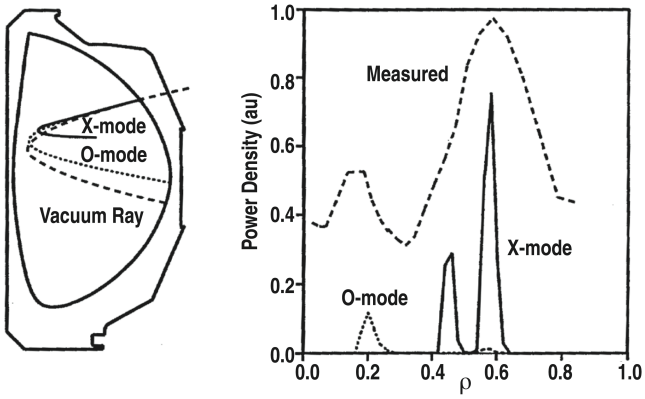

Fig. 1. (a) Projection of vacuum (dashed), X mode (solid), and O mode (dotted) ray trajectories onto a poloidal cross section of the DIII-D tokamak. The outer line shows the location of the plasma-facing components and the inner line shows the last closed flux surface of the plasma. (b) Comparison of the EC power deposition profile for X mode (solid) and O mode (dotted) with the response of the electron temperature measured by ECE to the modulation of the EC power (dashed). Reprinted from [10] by permission.

where

$$\gamma \equiv 1/\sqrt{1-\left(v/c\right)^2}$$

[7]. Even without putting momentum into the plasma, the waves can drive current due to the asymmetry [12]. Precise prediction of the plasma response, in this case the total current or the local current density, requires an accurate theory of the propagation, absorption, and the dynamics of the electrons in the plasma. The generation of current through ECCD has been demonstrated on several devices. Figure 2 shows a particularly clear example from the TCV tokamak where the ECCD is responsible for current greater than the total plasma current [13]. The total current is under feedback control, using the inductive drive as the actuator. The overdrive from ECCD results in the inductive current reversing sign to oppose the increase in current that would result if the feedback were not applied. This is evidenced by the negative voltage at the plasma surface and the change in sign of the current in the primary of the inductive transformer.

Quantitative validation of the ECCD theory is shown by examples from the DIII-D tokamak in Figure 3. The left figure compares the total current driven by ECCD to that predicted by the most accurate method — a relativistic Fokker-Planck calculation of the distribution function, including a momentum-

conserving collision operator and the remaining parallel electric field [14]. The agreement between theory and experiment is generally within the experimental uncertainties. The right figure compares the current density profile measured during ECCD with the theoretical prediction of the Fokker-Planck calculation [15]. Again, given the experimental accuracy possible, the measurement agrees well with the theoretical prediction. Including examples from other experiments and extensive benchmarking of codes [16], there is a high degree of confidence in the predictive theory of EC wave physics.

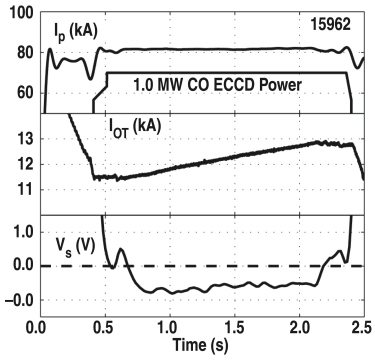

Fig. 2. Plasma with ECCD greater than the preset feedback value for plasma current from the TCV tokamak. Shown are time histories of the plasma current and EC power (upper box), current in the solenoid (middle box), and voltage at the plasma boundary (bottom box). Note the suppressed zero in the upper two boxes. Reprinted from [13] by permission.

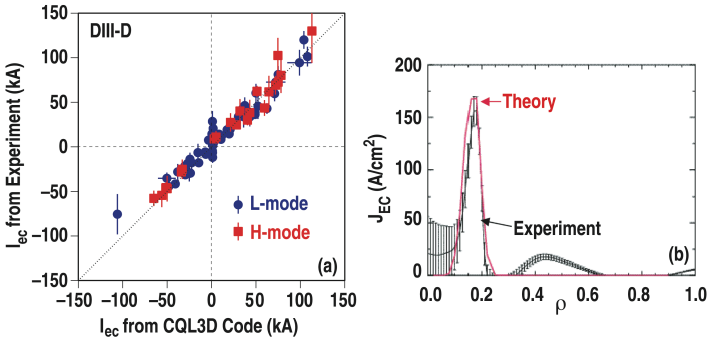

Fig. 3. (a) Comparison of measured current driven by ECCD to that predicted by a quasi-linear Fokker-Planck calculation with the experimental density, temperature, and impurity profiles including the effects of inductive parallel electric field. Reprinted from [14] by permission. (b) Comparison of measured current density profile from ECCD to that predicted by a quasi-linear Fokker-Planck calculation. Reprinted from [15] by permission.

3. Access to Steady-State Operating Conditions

The first general issue for steady-state operation of magnetic confinement fusion devices is accessing the relevant operating conditions. Initiation of the plasma and heating it to the necessary pressure for fusion energy are generic requirements for stellarators and tokamaks. For the tokamak, achieving the necessary pressure while maintaining high-energy gain is expected to require access to the high-confinement mode or "H mode" regime. This regime has certain access conditions. Stellarators have also observed H mode, but it is not clear that this is necessary or even beneficial for stellarator operation. Finally, for the tokamak, only certain classes of current profiles will support steady-state operation at high gain, and these profiles must be formed prior to going to the high temperature conditions associated with fusion energy because redistribution of current in plasmas of power plant size and temperatures has a time scale of 100s of seconds and might require capacity much greater than needed to sustain the steady-state. These topics will be examined here in turn.

Stellarators have relied on EC waves to initiate the plasma for many years [11]. Since the vacuum magnetic configuration usually is able to confine plasma, it is necessary simply to have a means to breakdown the neutral gas and accelerate the electrons sufficiently to build more plasma [17]. At the fundamental resonance ($f = f_{ce}$), EC waves can easily do this. At second harmonic ($f = 2f_{ce}$), it is perhaps surprising that EC waves can be sufficiently absorbed because absorption at higher harmonics is attributed to finite Larmor radius effects [9]. But many devices have shown that startup with second harmonic EC waves is effective, even with oblique launch and the corresponding reduced absorption [17–21]. Beyond the generation of the plasma, sufficient power must be available to overcome the radiation due to low charge states of impurities in the device (typically carbon and oxygen). The radiation is strongest for electron temperatures below 100 eV since higher temperatures lead to higher charges states and eventually fully ionized atoms that no longer radiate through line radiation. This phenomenon is known as "burnthrough" and is greatly facilitated by the EC wave power absorbed in the formation phase. This is especially critical for the next generation of tokamaks that will have superconducting coils. These new machines will have much lower inductive electric fields than present-day tokamaks due to limits on the voltages that can be applied to the coils and the significant shielding they require from the neutrons generated through the fusion reactions. Since plasma current is necessary for confinement, the tokamak must achieve burnthrough promptly or

the plasma current will decay away. The demonstrated ability to achieve burnthrough at low electric field on present-day experiments using EC assist [22,23] gives assurance that future tokamaks will be able to start up reliably at low electric field.

Bringing the plasma to sufficient pressure that the self-heating from fusion products (α particles in the case of deuterium-tritium fusion) becomes significant is essential to fusion energy production at high gain. The stellarator community envisions an operational point without auxiliary heating (ignited operation) [2], while steady-state tokamaks will require some level of auxiliary heating and current drive to maintain the magnetic configuration. In either case, auxiliary heating must be applied to start the fusion burn. The physics basis for predicting the amount of power required for tokamaks is based largely on experiments using injection of neutral beams (NBI) at energies higher than the thermal plasma temperature [24]. This form of heating has some similarity to heating by the α particles (transfer of energy through collisions), but also some significant differences (correlated particle source, possibility of correlated torque applied, energy transfer can be dominantly to ions in present experiments). The prediction of the power requirement is largely done using 0-D scalings derived from regression analysis of data from multiple experiments. Heating with EC waves does not have correlated particle or torque sources and the time scale for collisional coupling is two orders of magnitude shorter than for NBI, so the possibility of different power requirements in the EC case must be investigated. Since EC startup has been used extensively on stellarators, the standard scalings derived for stellarators have a significant fraction of the data from ECH [25,26]. No clear difference in the power requirements for different heating schemes is seen in these stellarator databases; however, the stellarator configuration strongly damps rotation that would arise from any applied torque. For tokamaks, the standard scalings [24,27] are heavily dominated by data from NBI. Figure 4 shows confinement data from EC heating of the FT-U tokamak plotted against the multi-tokamak database [28]. Within the accuracy of a log-log plot, the ECH data appears to agree well with the other data. However, the plasma in this dataset are not in the H mode confinement regime needed for fusion energy from steady-state tokamaks. As will be discussed below, there is no problem with access to H mode with ECH, but the lack of experimental data with EC systems on a scale comparable to the neutral beam heating systems on present-day tokamaks is of concern. The limited H mode data with EC agree well with the standard H mode scaling; it is of great interest to see whether this

agreement continues into the regime where strong NBI implies significant core fueling and applied torque.

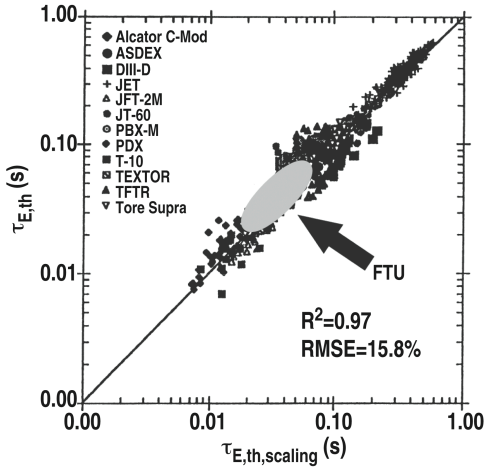

Fig. 4. Thermal confinement time from ECH plasmas in the FT-U tokamak plotted against the ITER-97L scaling [29]. Reprinted from [28] by permission.

In tokamaks, access to the H-mode confinement regime is characterized by crossing a threshold level of power flowing through the plasma boundary [30]. ECH is effective at accessing the H-mode regime [31] and recent experiments confirm that the access conditions are similar for EC and NBI [32]. Figure 5 shows data from the AUG tokamak indicating that the power required to access H mode is the same within the uncertainties of the experimental data. It also shows one advantage of ECH — the absence of NBI data at low density is due to restrictions on NBI operation at low density. It is possible to use ECH at lower densities where the transparency of the plasma to the neutral beam excludes its application. In this case, there is little advantage to the lower density operation, because the power threshold increases again. The scaling of the minimum density is not known, so there may be a clear advantage at low density for ECH in future tokamaks. H mode has been observed in stellarators first with ECH [33]. Figure 6 shows time histories from the WVII-AS stellarator where H mode is obtained with ECH as the sole heating source. There appears to be no power threshold for H mode access in the WVII-AS stellarator; instead, there is a requirement on the configuration. It is not clear whether H mode is an advantage to stellarators — present conceptual designs of power plants do not

make use of it, despite the need for improvement of stellarator confinement — but the capability for H mode operation exists and was discovered using ECH.

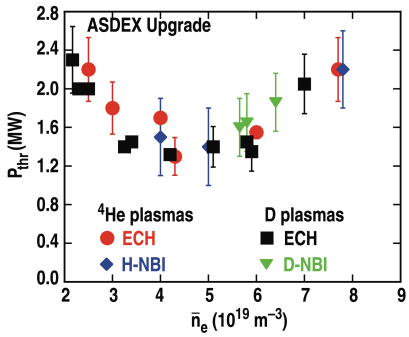

Fig. 5. Threshold power for entering H mode in the AUG tokamak using ECH and NBI in helium and deuterium plasmas as a function of line-averaged density. Reprinted from [32] by permission.

The last topic relevant to accessing steady-state operation discussed here is formation of the desired current profile. This issue is specific to the steady-state tokamak. At constant total plasma current, the profile of the inductive current density in the tokamak will diffuse toward a profile consistent with a constant electric potential in radius and the conductivity profile, which is normally very peaked ($\propto T_e^{3/2}$). The total current density profile will vary during this time in proportion to the local fraction of inductive current. A broad current profile is favored for steady-state tokamak operation [1], both because it implies a substantial bootstrap current at the edge (large noninductive fraction) and it is favorable for stability in the wall-stabilized regime. The large difference between the "natural" profile toward which inductive current density evolves and the desired profile for steady-state tokamak operation motivates using the current rise phase of the discharge to "steer" the current profile toward the desired value [34]. The current rise phase has several clear advantages for this task. First, the inductive drive supplies current from the edge, so the profiles are naturally broad during this time. The power from the external heating dominates the power balance during this time, whereas at current flattop the fusion self-heating can be large. The lower temperatures during the current rise phase allow modifications of the profile on a shorter time scale. Finally, keeping the plasma close to the desired stable current profile avoids the need to make large changes in the current profile, which might lead to ideal or resistive instabilities during the transition.

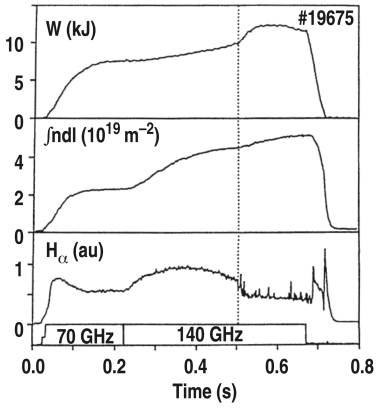

Fig. 6. Time histories of the stored energy (top), line-integrated density (middle), and edge D_α emission (bottom) from a plasma with a transition to H mode using ECH in the WVII-AS stellarator. The bottom figure shows the timing of the application of the two different ECH systems. The dotted vertical line indicates the time of the transition to H mode. Reprinted from [33] by permission.

ECH is an ideal tool for profile modification, especially under feedback control, since it can be localized in both space and time. Two examples of feedback control are given here. On the TCV tokamak, the power applied to two fixed radial locations has allowed feedback control of the electron temperature profile [35]. Figure 7 shows how the peak value and the profile width, defined as the fraction of the simple profile average to the peak value, are controlled to match target waveform values by varying the power at normalized radii of 0.2 and 0.5. The feedback algorithm has been specifically designed for this application. Modeling of the plasma dynamics allows the system to follow rapid changes in the target values without overshoot or undershoot as long as the required power is in the range available to the system. On the DIII-D tokamak, the EC power at a single radial location near the half radius has been used to modify the electric conductivity during the current ramp to feedback control the value of the central safety factor $q(0)$ [36]. A real-time estimate of $q(0)$ is provided to the feedback system through inclusion of the motional Stark effect (MSE) measurements of the internal vertical magnetic field in the real-time equilibrium reconstructions. A proportional-integral gain controller is used to determine the ECH power using the simple model that more power (hotter plasma) slows the reduction in $q(0)$. Therefore, if the measured value falls below the target value more power is applied to slow the downward evolution (and

vice versa). Again, this controller does a reasonable job of providing a $q(0)$ evolution that follows the target trajectory until the requested power encounters the system limits. Note that in the context of tailoring the current profile during the current rise, both the TCV and DIII-D schemes act on the conductivity — the ECCD is much less than the inductive current and is not effective at modifying the current profile. More sophisticated feedback schemes are being tested that take into account the expected plasma response and schedule the future actuator trajectories [34].

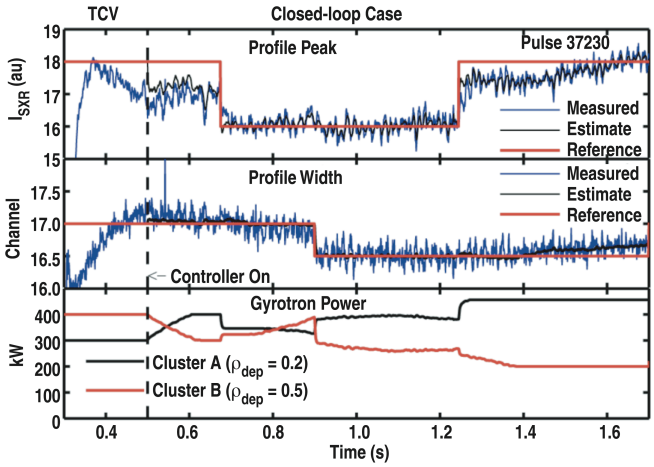

Fig. 7. Time histories of peak soft x-ray intensity (top), the normalized average soft x-ray intensity (middle), and the ECH power in two separate systems aimed at a normalized radius of 0.2 (blue) and 0.5 (red), respectively (bottom). The red lines in the top boxes indicate the reference value input to the controller. Reprinted from [35] by permission.

4. Sustaining the Steady-State Regime

As discussed earlier, the present vision for stellarator power plants is to operate in the ignited regime, where the self-heating sustains the pressure in a magnetic configuration determined largely by the external coil set. Given this view, there is no need for ECH or ECCD in routine operation. In the next section, a possible role for fine tuning the operating point of a stellarator with ECCD will be discussed. For the steady-state tokamak, however, ECCD is envisioned to play a critical role in maintaining the current profile noninductively in a stable configuration.

As shown above, experiments have demonstrated full sustainment of the current profile in a tokamak by ECCD. However, sustaining the total current by external sources at the expected parameters for power plant operation is not practical. The current drive efficiencies are too low by about a factor of 2.5 to allow economic operation, due to the large fraction of the electrical output of the plant that would need to be recirculated to power the current drive systems. (See Ref. 1 for a more complete discussion of this point.) This necessitates that the self-generated "bootstrap" current [37] must dominate the current generation. But this current is not likely to yield full current drive nor perhaps a stable current profile on its own. Here is where the flexibility of the ECCD to supply current at various radii and magnitudes is essential to steady-state operation. The ECCD can be deployed to make up the difference locally between the desired total current density profile that is stable to ideal and resistive instabilities at the desired operating pressure and the bootstrap current profile that is largely dependent on the shape of the density and temperature profiles.

An example of ECCD used in this role from the DIII-D tokamak is shown in Fig. 8 [38]. The fraction of current generated noninductively is sustained at 100% for nearly 1 s [Fig. 8(a)], which is still less than a global resistive relaxation time for this plasma. The duration is limited by the technical limitations of the NBI system and not plasma effects in this case. The fact that the current profile is not yet in equilibrium is clear from the fact that the remaining inductive current still has some spatial structure [Fig. 8(b)]. The calculated noninductive currents [Fig. 8(c)] show that the dominant noninductive current is the bootstrap current at all radii. The edge current is exclusively bootstrap current, while the NBCD and ECCD contribute significantly in the plasma interior. The ECCD is not positioned to maximize the driven current, but to optimize stability to tearing modes and drive current to make up the difference between the sum of the bootstrap current and the NBCD. In the case shown, it appears that the combination of current sources is nearly optimal for sustaining the current noninductively when the inductive current equilibrates.

The optimization of the ECCD distribution has been done empirically, as there is no equivalent to the ideal MHD codes for surveying large numbers of equilibria for tearing stability. An example of this optimization is shown in Figure 9. Identical target plasmas are made with only the three variations in the ECCD profile shown [Fig. 9(c)] — two profiles with very narrow deposition at two locations and one profile with broad deposition spanning the region of the two narrow cases. At β_N=3.2, the plasma is stable to n=1 tearing modes for the

duration of the high performance phase. At β_N=3.4, however, the two narrow deposition cases are unstable, while the broad deposition case remains stable. In general, broad ECCD deposition results in stability to *n*=1 tearing modes at higher β_N in DIII-D.

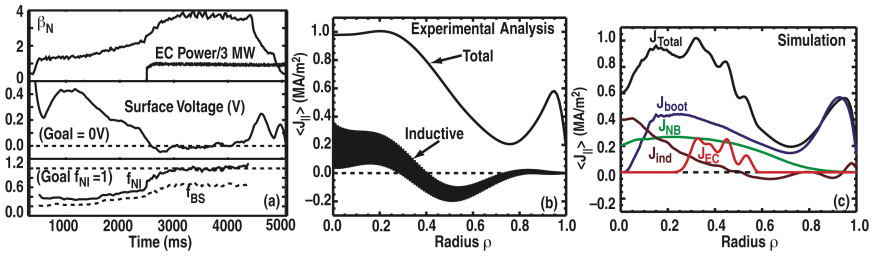

Fig. 8. (a) Time histories of normalized pressure (β_N) and EC power (top), surface inductive voltage (middle), and noninductive current fraction (solid) and bootstrap current fraction (dashed) (bottom). (b) Radial profiles of the flux-surface average current density and the inductive current density inferred from experimental equilibrium reconstructions. (c) Radial profiles of components of the current density calculated from modeling (bootstrap (blue), NBCD (green), inductive (brown), ECCD (red)) and the total current density (black). Reprinted from [38] by permission.

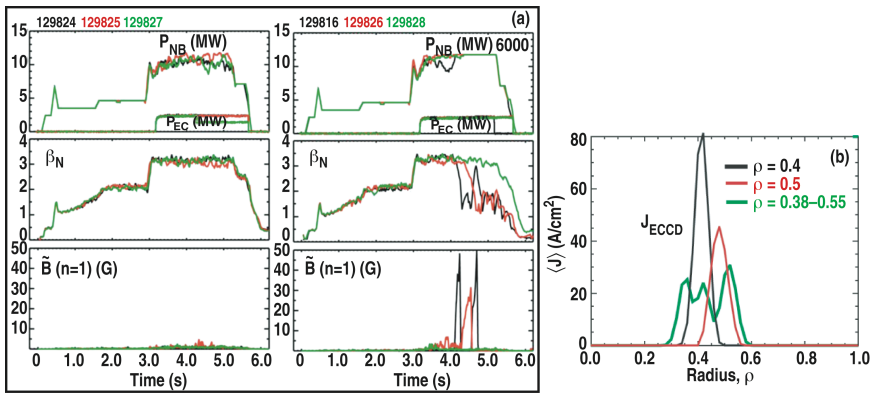

Fig. 9. (a) Time histories of NBI and EC power (top), normalized pressure (β_N) (middle), and *n*=1 magnetic fluctuation amplitude at the vacuum vessel (bottom) for three steady-state scenario plasmas at β_N = 3.2 with various ECCD spatial distributions. (b) Same as (a), but with β_N = 3.4. (c) Radial profiles of the ECCD current density showing the three different spatial distributions.

5. Control of the Operating Point

From the point of view of power plant operation, a steady-state scenario that has an operating point that is passively stable, i.e., it returns to the original

parameters after small perturbations without external intervention, is an optimal solution. Solutions like this seem reasonable for stellarators, since there is little free energy in the magnetic configuration and stellarator power plants are being designed to lie on the stable part of the fusion power curve to perturbations in temperature. They will need to be continuously fueled, however, and may require some feedback control of the heating due to the refueling process, depending on the method used. Depending on the type of stellarator and the sensitivity of the plasma transport to details of the internal magnetic configuration, some tuning of both the pressure and the magnetic configuration may be needed to remain at the desired operating point. ECH and ECCD are unique tools to allow local tuning, and due to the ability to act locally, they should be able to carry out this control with minimum impact on the energy gain.

As an example, Fig. 10 shows the sensitivity of the W7-X divertor design to the details of the magnetic configuration [39]. The divertor is designed to handle the heat and particle fluxes in the 3-D magnetic geometry. However, it is fixed in space and optimized for a given configuration, taking advantage of the proximity of a low-order rational surface to increase the "wetted" area in the divertor to reduce the heat flux. The simulation shown compares the magnetic configuration in vacuum to that with full operating pressure. A relatively small amount of current (43 kA) due to the bootstrap current changes the magnetic configuration in the divertor region significantly [left side of Fig. 10]. The same EC system that is used to increase the pressure to the operating point can be used to compensate temporarily the bootstrap current and restore the proper magnetic configuration for the divertor until the coil currents can be changed to do this in steady state. (The deposition of the ECCD is not optimized in radius in the case shown, leading to magnetic shear inside the plasma that is probably undesirable. It is expected that this can be further optimized.)

While this simulation was done in the context of accessing the desired operating point in W7-X, the same general issues can be anticipated at the operating point of a stellarator power plant with similar design philosophy. If the divertor has been optimized for a particular magnetic configuration, then perturbations away from this optimized configuration must be rapidly dealt with in order to preserve the integrity of the divertor in the presence of full-performance heat fluxes in this non-optimized state. The large inductances and low voltage limits on the superconducting coils expected for steady-state power plants imply a more rapid response is needed. A rapid compensation system with ECCD to restore temporarily the magnetic configuration seems much more

desirable that a full unscheduled shutdown and could maintain the fusion power output at a reasonable level with only a temporary reduction of gain. Experiments on the WVII-AS stellarator showed the ability of ECCD to compensate the bootstrap current globally as part of a larger experiment to validate the theoretical model of ECCD in that configuration [40].

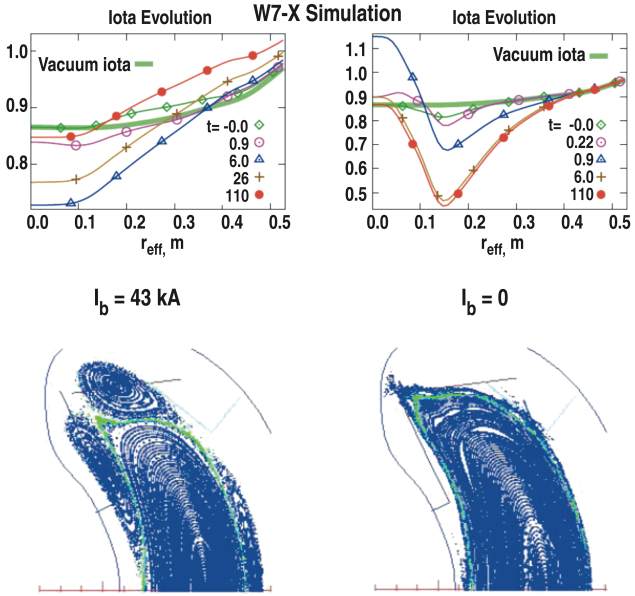

Fig. 10. The upper figures show the vacuum ι profile for the case without (left) and with (right) correction for the net bootstrap current with ECCD. The lower figures are Poincaré plots at a single poloidal cross-section showing the effect of each case on the magnetic configuration in the divertor region.

For tokamaks, a passively stable operating point may be possible, but it is much less likely to exist against all perturbations, due to the strong coupling of the pressure and current profiles through the bootstrap current and the large free energy in the plasma current required to sustain the magnetic configuration. The most critical control task is to stabilize the operating point following a perturbation to allow an orderly shutdown and restart of the plasma, rather than activation of the protection systems required for rapid shutdown. Again ECCD has a proven ability to control instabilities in present-day tokamaks that appears to be transferable in both physics and technology to future uses.

Control of MHD instabilities by precise localization of ECCD under feedback control has been demonstrated in several experiments. Tearing modes are a significant concern for steady-state tokamaks, as they can alter the magnetic configuration and the energy confinement significantly and, if not dealt with, can lead to a complete loss of thermal and magnetic stored energy (disruption). Several experiments have demonstrated suppression of tearing modes by ECCD deposited precisely in the magnetic islands generated by the tearing modes [41]. Experiments on JT-60U [42] have demonstrated automated detection of tearing modes using an electron cyclotron emission (ECE) diagnostic and subsequent suppression by feedback control using an EC launcher with a steerable mirror (Fig. 11). This technology seems feasible for use in a power plant. Other experiments have used plasma motion or change in the toroidal magnetic field to demonstrate the feasibility of feedback control, but these methods are not amenable to the power plant environment. Pre-emptive stabilization has been demonstrated as a possible means of enhanced operation by active feedback control [43]. Experiments on Tore Supra demonstrated control of the sawtooth instability by means similar to the JT-60U tearing mode experiment [44]. While the sawtooth instability is unlikely to be encountered in steady-state tokamak operation, the proof of principle of ECCD for feedback control of MHD instabilities bolsters the physics and technology basis needed for future tokamaks.

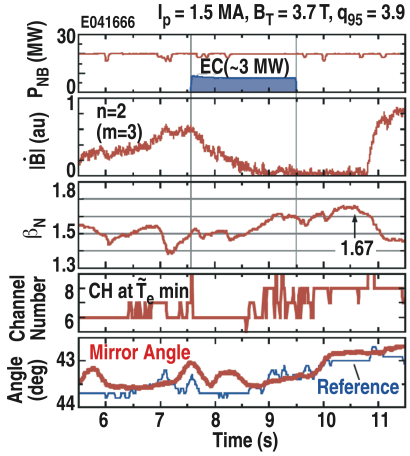

Fig. 11. Time histories of (a) NB and EC power, (b) *n*=2 magnetic fluctuations at the vacuum vessel, (c) normalized pressure (β_N), (d) ECE channel number for mode location, and (e) aiming mirror command and response for a plasma from the tearing mode suppression by ECCD experiment on the JT-60U tokamak. Reprinted from [42] by permission.

Fusion power plants are likely to have plasma-facing components made from high-Z materials, such as tungsten. If these metals get into the core of the plasma, they can radiate copious quantities of energy, cooling the plasma and spoiling the fusion output. In extreme cases, a radiative collapse could lead to disruption. The optimal solution is a divertor design that keeps these high-Z impurities out of the plasma. However, it is necessary to anticipate off-normal events that may bring these metals into the plasma. The AUG tokamak has nearly complete coverage of the plasma-facing components with tungsten. Accumulation of tungsten at the plasma center can be mitigated by localized ECH [45]. By scanning the location of the ECH from plasma center to off-axis, the sensitivity to the heating location is clear (Fig. 12). The concentration of tungsten rises exponentially once the heating moves to a relatively small radius off-axis. Similar dependence on ECH deposition location is seen in scans of the toroidal magnetic field, which move the resonance in major radius. A validated physical model for this behavior is not yet available.

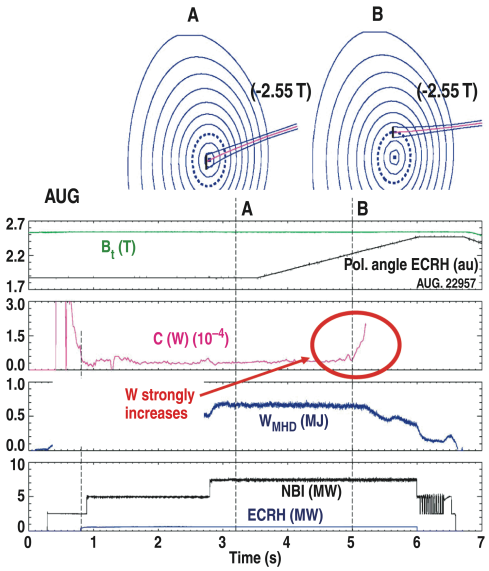

Fig. 12. Time histories of (a) toroidal field magnitude and poloidal angle of the EC aiming mirror, (b) tungsten concentration, (c) stored energy, and (d) NB and EC powers for a scan of the EC heating deposition location. The cross-sections above labeled A and B show the heating location of the EC at the corresponding vertical lines in the time histories. Reprinted from [45] by permission.

6. Prospects for Use of ECH and ECCD in Fusion Energy Devices

The energy gain in magnetic fusion devices scales strongly with magnetic field [46]. This motivates power plant designers to operate at the maximum field allowed by the superconducting materials from which the magnets are likely to be made. Present superconducting materials limit the central vacuum field in fusion devices to ≤7 T, which implies a fundamental cyclotron resonance frequency of <200 GHz. This frequency is only slightly above that of the presently developed high-power cw gyrotron sources (≤170 GHz). The electron plasma frequency, which sets the wave cutoff for the O mode, is ~5×10^{20} m^{-3}. A simple estimate using $\langle\beta\rangle = 5\%$ as a typical value for the operational point of a fusion power plant implies that the operating density will be below the O mode cutoff, independent of B, if $\langle T\rangle > 6$ keV, which is likely due to the increase in fusion power faster than the square of the temperature in this range (trading density for temperature at fixed β increases fusion power). This argument indicates ECH and ECCD are viable tools for fusion power plants.

A secondary advantage for ECH and ECCD systems is the high power density possible in the transmission lines. Power densities up to 1 GW/m^2 have been demonstrated in evacuated transmission line [47]. This high power density allows substantial power to be applied without a corresponding decrease in the breeding blanket and shielding area of the fusion device. The ability to guide the power with transmission lines also has a very limited impact on the coil design, which is especially critical for stellarator systems that can have complex 3-D coil sets. Other heating and current drive schemes under consideration for fusion power plants have more significant impact on the design of the physical plant.

These considerations, in addition to the proven abilities of ECH and ECCD to deliver functions essential to steady-state operation, have led to the inclusion of EC systems in the design of the next-step fusion experiments and consideration in the design for power plant demonstration facilities. The next large stellarator, W7-X, has EC as a primary heating system and allows for the possibility of ECCD [48]. An EC system is already in use on LHD [49], the largest operating stellarator in the world. The JT-60SA tokamak, which aims at demonstration of conditions necessary for steady-state operation, employs an EC system for heating and current drive [50]. The ITER tokamak, envisioned to be the first demonstration of burning plasmas in steady-state conditions, also has an EC system as one of its primary auxiliary heating and current drive systems [46]. Two potential steady-state scenarios that use ECCD as a essential element are shown in Fig. 13. The upper case is a simulation, based on the DIII-D

scenario shown in Fig. 8, that approaches the ITER physics objective of steady-state operation with fusion energy gain Q of 5 [1]. The role of ECCD in this case is to supply off-axis current drive to obtain fully noninductive operation with min(q) > 1. The lower case takes advantage of the local ECCD to induce a transport barrier (due to the form of the energy transport model used) to generate significant bootstrap current in addition to the off-axis ECCD. (This simulation is similar to those published results that include lower hybrid current drive [51]). Both types of scenarios are under study in present-day experiments. These simulations indicate that EC systems may play a critical role in meeting the ITER physics objective of steady-state operation with Q=5.

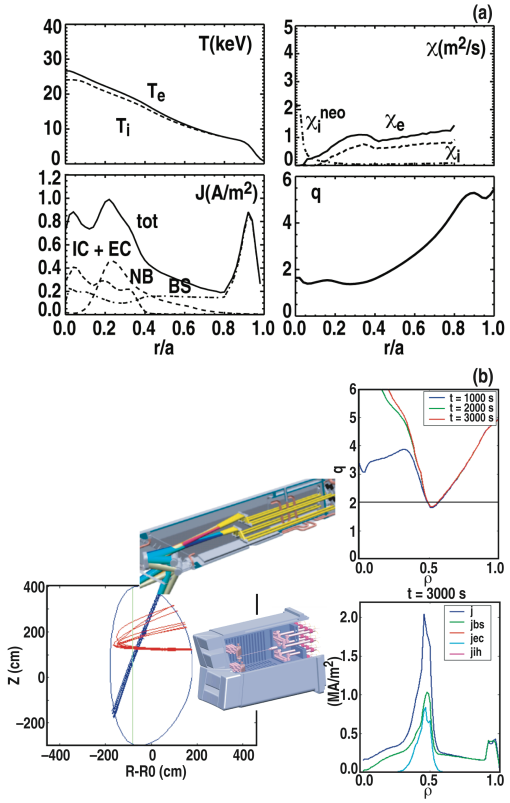

Fig. 13. Upper boxes show the temperature, diffusivity, current density, and q profiles from a simulation of an ITER steady-state scenario based on a DIII-D plasma. Reprinted from [1] by permission. Lower boxes show the q and current density profiles from a simulation of ITER steady-state scenario based on a model allowing formation of a transport barrier.

7. Conclusions

The evidence presented here indicates that ECH and ECCD can perform vital roles for steady-state magnetic fusion energy systems, from accessing the desired operating conditions to sustaining those conditions and controlling the operating point. In some cases such as flexible off-axis current drive and instability control, these roles are uniquely possible for EC systems — no other means are known. These unique capabilities, along with the technological advantages of EC systems and the proven technology developments over the past decades, enhance the prospects for steady-state fusion energy systems.

Acknowledgments

This work was supported by the U.S. Department of Energy under DE-FC02-04ER54698.

References

[1] T.C. Luce, "Realizing Steady-State Tokamak Operation for Fusion Energy," submitted to Phys. Plasmas (2010).
[2] F. Najmabadi, et al., *Fusion Sci. Technol.* **54**, 655 (2008).
[3] J.P. Freidberg, *Rev. Mod. Phys.* **54**, 801 (1982).
[4] N.J. Fisch, *Rev. Mod. Phys.* **59**, 175 (1987).
[5] K. Sakamoto, these proceedings (2010).
[6] T.H. Stix, *Waves in Plasmas*, 2nd ed., AIP Press, New York (1992).
[7] R. Prater, *Phys. Plasmas* **11**, 2349 (2004).
[8] S. Weinberg, *Phys. Rev.* **126**, 1899 (1962).
[9] M. Bornatici, et al., *Nucl. Fusion* **23**, 1153 (1983).
[10] C.C. Petty, et al., Radio Frequency Power in Plasmas, *AIP Conf. Proc.* **485**, AIP, Melville, NY (1999) p. 245.
[11] V. Erckmann and U. Gasparino, *Plasma Phys. Control. Fusion* **36**, 1869 (1994).
[12] N.J. Fisch and A.H. Boozer, *Phys. Rev. Lett.* **45**, 720 (1980).
[13] O. Sauter, et al., *Phys. Rev. Lett.* **84**, 3322 (2000).
[14] C.C. Petty, et al., *Nucl. Fusion* **42**, 1366 (2002).
[15] L.L. Lao, et al., in Radio Frequency Power in Plasmas, *AIP Conf. Series* **595**, 310 (2001).
[16] R. Prater, et al., *Nucl. Fusion* **48**, 035006 (2008).
[17] G.L. Jackson, et al., *Nucl. Fusion* **47**, 257 (2007).
[18] B. Lloyd, et al., Proc. 13th European Conf. (Schliersee) vol 10C part II (European Physical Society) 266 (1986).
[19] Zhan R. et al., *Int. J. Infrared Millimeter Waves* **11,** 765 (1990).
[20] K. Kajiwara, et al., *Nucl. Fusion* **45,** 694 (2005).

[21] Y.S. Bae, et al., *Nucl. Fusion* **49**, 022001 (2009).
[22] G.L. Jackson, et al., *Nucl. Fusion* **48**, 125002 (2008).
[23] A.C.C. Sips, et al., *Nucl. Fusion* **49**, 085015 (2009).
[24] ITER Physics Basis Editors, et al., *Nucl. Fusion* **39**, 2175 (1999).
[25] U. Stroth, et al., *Nucl. Fusion* **36**, 1063 (1996).
[26] H. Yamada, et al., *Nucl. Fusion* **45**, 1684 (2005).
[27] P.N. Yushmanov, et al., *Nucl. Fusion* **30**, 1999 (1990).
[28] S. Cirant, et al., *Plasma Phys. Control. Fusion* **41**, B351 (1999).
[29] S.M. Kaye, et al., *Nucl. Fusion* **37**, 1303 (1997).
[30] J.A. Snipes, et al., *Nucl. Fusion* **36**, 1217 (1996).
[31] John Lohr, et al., *Phys. Rev. Lett.* **60**, 2630 (1988).
[32] F. Ryter, et al., *Nucl. Fusion* **49**, 062003 (2009).
[33] V. Erckmann, et al., *Phys. Rev. Lett.* **70**, 2086 (1993).
[34] Y. Ou, et al., *Plasma Phys. Control. Fusion* **50**, 115001 (2008).
[35] J.I. Paley, et al., *Plasma Phys. Control. Fusion* **51**, 124041 (2009).
[36] J.R. Ferron, et al., *Nucl. Fusion* **46**, L13 (2006).
[37] J. Wesson, D.J. Campbell, *Tokamaks*, 3rd ed., Oxford University Press, Oxford, UK, 2004.
[38] C.T. Holcomb, et al., *Phys. Plasmas* **16**, 056116 (2009).
[39] H. Maaßberg, private communication (2010).
[40] V. Erckmann et al., *Fusion Eng. Design* **53**, 365–375 (2001).
[41] R.J. La Haye, *Phys. Plasmas* **13**, 055501 (2006).
[42] A. Isayama, et al., *Nucl. Fusion* **43**, 1242 (2003).
[43] R. Prater, et al., *Nucl. Fusion* **47**, 371 (2007).
[44] M. Lennholm, et al., *Fusion Sci. Technol.* **55**, 45 (2009).
[45] J. Stober, et al., these proceedings (2010).
[46] C. Gormezano, et al., *Nucl. Fusion* **47**, S285 (2007).
[47] T.C. Luce, *IEEE Trans. Plasma Sci.* **30**, 734 (2002).
[48] T. Klinger, "The Construction of the W7-X Stellarator," Proc. 22nd IAEA Fusion Energy Conf., Geneva, http://www-naweb.iaea.org/napc/physics/FEC/FEC2008/papers/ft_1-4.pdf.
[49] S. Kubo, et al., these proceedings (2010).
[50] T. Fujita, et al., *Nucl. Fusion* **47**, 1512 (2007).
[51] J. Garcia, et al., *Phys. Rev. Lett.* **100**, 255004 (2008).